Journal of Biomechanics 44 (2011) 2558–2564

Contents lists available at ScienceDirect

Journal of Biomechanics

journal homepage: www.elsevier.com/locate/jbiomech
www.JBiomech.com

Probing softness of the parietal pleural surface at the micron scale

Jae Hun Kim [a,*], James P. Butler [a,b,c], Stephen H. Loring [a]

[a] Department of Anesthesia, Critical Care and Pain Medicine, Beth Israel Deaconess Medical Center and Harvard Medical School, 330 Brookline Ave., Dana 715, Boston, MA 02215, USA
[b] Molecular and Integrative Physiological Sciences, Harvard School of Public Health, 665 Huntington Avenue, Boston, MA, USA
[c] Division of Sleep Medicine, Department of Medicine, Harvard Medical School and Brigham and Women's Hospital, Boston, MA, USA

ARTICLE INFO

Article history:
Accepted 6 July 2011

Keywords:
Parietal pleura
AFM
Hertzian indentation
Elastohydrodynamic lubrication
Rat

ABSTRACT

The pleural surfaces of the chest wall and lung slide against each other, lubricated by pleural fluid. During sliding motion of soft tissues, shear induced hydrodynamic pressure deforms the surfaces, promoting uniformity of the fluid layer thickness, thereby reducing friction. To assess pleural deformability at length scales comparable to pleural fluid thickness, we measured the modulus of the parietal pleura of rat chest wall using atomic force microscopy (AFM) to indent the pleural surface with spheres (radius 2.5 and 5 μm). The pleura exhibited two distinct indentation responses depending on location, reflecting either homogeneous or significantly heterogeneous tissue properties. We found an elastic modulus of 0.38–0.95 kPa, lower than the values measured using flat-ended cylinders >100 μm radii (Gouldstone et al., 2003, Journal of Applied Physiology 95, 2345–2349). Interestingly, the pleura exhibited a three-fold higher modulus when probed using 2.5 vs. 5 μm spherical tips at the same normalized depth, confirming depth dependent inhomogeneous elastic properties. The observed softness of the pleura supports the hypothesis that unevenness of the pleural surface on this scale is smoothed by local hydrodynamic pressure.

1. Introduction

During respiratory motion, the pleural surfaces of the lung and chest wall slide reciprocally relative to each other. Pleural fluid facilitates this, but the nature of pleural lubrication has been controversial. Agostoni (1986) attributed the difference between pleural fluid pressure and lung surface pressure to points of contact between surfaces, suggesting boundary lubrication. This requires normal loads being partially supported by contacts at surface asperities, depending on the roughness and stiffness of the pleural surfaces. In an opposing view, Lai-Fook and Kaplowitz (1985) argued that a continuous fluid layer separates the pleural surfaces, implying elastohydrodynamic lubrication. Lai-Fook (2004) maintains that pleural liquid pressure is equal to pleural surface pressure.

In elastohydrodynamic lubrication, sliding of soft uneven surfaces generates hydrodynamic pressure, which smoothes roughness and redistributes fluid from thick to thin fluid regions, promoting a more uniform fluid layer (Dowson and Jin, 1986; Lai et al., 2002; Butler et al., 1995). Computational work based on fluid dynamic models shows that the pressure distribution depends on the roughness wavelength and the elastic properties of the surface (Gouldstone et al., 2003a; Moghani et al., 2009). Microscopic studies of quick-frozen chests reveal pleural surface asperities with widths ranging from tens to hundreds of microns (Albertine et al., 1991). The degree to which these asperities are smoothed by hydrodynamic forces and thus the likelihood that elastohydrodynamic lubrication characterizes pleural tribology depends critically on the value of the elastic moduli of the pleural surfaces. Analytic and parametric studies show that the tissue softness enhances the lifting force during sliding, thus increasing the minimum fluid thickness (Butler and Loring, 2008; Skotheim and Mahadevan, 2005). Importantly, maintaining a uniform liquid thickness requires pleural deformation at length scales comparable to the fluid layer itself.

The elasticity of pleural tissues, which represents a measure of surface deformability, has been measured using indentation techniques (Lai-Fook et al., 1976; Hajji et al., 1979; Gouldstone et al., 2003b). These measurements have employed probes much larger than the pleural fluid thickness of ~8–20 μm (Lai-Fook and Kaplowitz, 1985); the elasticity of the pleural surface at length scales comparable to fluid thickness is currently unknown.

To fill this gap, we used atomic force microscopy (AFM) to probe tissue at the micron scale in a physiologic fluid environment (Drake et al., 1989). To avoid stress singularities associated with sharp AFM tips, we used 2.5 and 5 μm spherical tips to simulate in-vivo pleural deformations. Tissue elastic properties were determined from the AFM force/deflection data by fitting

* Corresponding author. Tel.: +1 617 667 5296; fax: +1 617 667 1500.
E-mail address: mbeads@hotmail.com (J.H. Kim).

0021-9290/$ - see front matter © 2011 Elsevier Ltd. All rights reserved.
doi:10.1016/j.jbiomech.2011.07.008

with Hertz's elastic model of homogeneous materials (Hertz, 1882). The effect of sphere size on the probed stiffness was interpreted on the basis of structural inhomogeneity of the pleura and subjacent tissue.

We found:

(1) The elastic modulus of the parietal pleura measured at the micron scale was two-fold to five-fold lower than the values previously obtained with flat probes of radii $>100\,\mu m$ (Gouldstone et al., 2003b).
(2) There were two characteristic indentation responses, Hertzian and non-Hertzian, reflecting homogeneous tissue properties and structural inhomogeneities.

2. Materials and methods

2.1. Tissue preparation

We used thirteen Sprague-Dawley rats (300–500 g) under a protocol approved by the Institutional Animal Care and Use Committee of Beth Israel Deaconess Medical Center. Each animal received heparin (5000 units i.p.), to prevent fibrin formation on the mesothelial surface, and was killed ~5 min later with an overdose of sodium pentobarbital (>200 mg/kg i.p.) (Lin et al. 2008). Immediately after death, the thoracic cavity was opened and the intercostal muscles and intervening ribs were excised en bloc (~4 mm × 4 mm × 2 mm) between the 3rd and 7th rib. To prevent abrasion, we avoided touching the parietal surfaces, and immersed the specimen in saline.

2.2. Atomic force microscopy

A commercial AFM (MFP-3D; Asylum, Santa Barbara, CA) was used with probes constructed with borosilicate spherical tips, nominal radius 2.5 and 5 μm, glued to triangular cantilevers with a nominal spring constant $k=0.06$ N/m (Novascan Technologies, Ames, Iowa). k was independently measured by the thermal noise method (Hutter and Bechhoefer, 1993; Butt and Jaschke, 1995; Stark et al., 2001). The laser detector was calibrated for zero force before each experiment. The piezotranslator extended and retracted the probe at 2 μm/s. Measurements were completed within 5 h after death. One specimen from each rat was used for these measurements. Ten to 100 force–displacement curves were collected from each rat, separated laterally by at least 5 and 10 μm for 2.5 and 5 μm tips, respectively. Maximum forces were ~4 nN.

2.3. Data analysis

From Hooke's law, force F is linearly related to deflection, $F=kd$, where d is the deflection of the cantilever. The indentation depth δ is the relative displacement of cantilever holder $(z-z_c)$ minus d, where z is the displacement of the piezo actuator and z_c is the contact point. The classical Hertz model for homogeneous material describes the force/depth relation for spherical punch indentations. For incompressible tissue and a probe of radius R this relation is

$$F=\frac{16ER^{1/2}}{9}\delta^{3/2}=\frac{16E}{9}a\delta \quad (1)$$

where E is Young's modulus, and a is the radius of contact between the punch and the surface (Hertz, 1882). In terms of z and d,

$$z-d-z_c=\left(\frac{9}{16ER^{1/2}}\right)^{2/3}F^{2/3} \quad (2)$$

From direct measurements of z and d, E can be extracted from Eq. (2) if z_c can be found.

Determination of z_c is nontrivial for soft tissues, because the initial deflection is small and nonlinear (Crick and Yin, 2007), and force–depth curves often do not show a clear transition when tip–tissue contact is made. We used least squares fitting rather than visual inspection or other methods for determining z_c and E (Lin and Horkay, 2008; Shoelson et al., 2004). Much of our data showed weak force increases over large depths, followed by progressive steepening, which we attributed to surface heterogeneity (Fig. 2b). To robustly detect initial force increase, we performed initial fitting in a small force window for the first guess of contact point, and searched iteratively for the best z_c. The left panel of Fig. 1 shows typical force–displacement data from approach (loading) and retraction (unloading). During retraction, negative and discontinuous forces were observed, a pattern characteristic of adhesion between the tip and the underlying tissue (Wojcikiewicz et al., 2003; Sen et al., 2005). This was not seen in the approaching phase, suggesting negligible adhesion artifacts. We therefore analyzed only approach curves. Initially, F *vs.* z data were fitted to the Hertz model over a range of forces from 0.2 to 0.8 nN, the latter approximating 20% of the maximum force at maximal indentation. The intersection between the fitted curve and the zero force line was picked as an initial guess of z_c. The force–displacement data were then fitted to the Hertz model over a range of depths (depth window) in the post-contact region and to zero force in the pre-contact region. z_c was then varied in 4 nm increments between 0.4 and 0.8 μm below and above the initial guess. The root mean squared error (RMS) was computed for each z_c guess, and the value of z_c that minimized the RMS was taken as the contact point (right panel of Fig. 1). E was recovered from Eq. (2), here referred to as overall stiffness E_o. Force and depth windows and sweep ranges of contact points for each probe are summarized in Table 1. By setting maximum normalized depths of the fitting windows equal, we ensured that the average strain was the same for all probes (see Appendix A).

After contact point analysis, the mean squared depth-wise error over the whole range of F vs. z data (RMS_{whole}) was computed for each curve, as an index of deviation from the homogeneous elastic model. Average E_o for each rat was determined after excluding the 10% of indentation curves with the highest RMS_{whole}. The averages from 10 rats for each probe were compared using unpaired two-tailed Student's t tests. In addition to E_o, E was computed at each data point according to Eq. 2, giving an apparent pointwise stiffness E_p at each indentation depth (Costa and Yin, 1999). Finally, the high force stiffness E_{hf} was computed over a force window (2–4 nN) (Domke and Radmacher, 1998) directly from the F vs. z curves, fitted to Eq. (2) without constraining z_c.

Table 1
Summary of fitting parameters used for determining contact point and stiffness.

	2.5 μm sphere	5 μm sphere
Force window for initial guess of contact point (nN)	0.2–0.8	0.2–0.8
Depth window $(z-z_c-d)$ (μm)	0.8	1.6
Sweep range of contact point (left/right) (μm)	0.4/0.4	0.8/0.8
Maximum normalized depth $(\delta_{max}/a_{max}=a_{max}/R)$	0.56	0.56

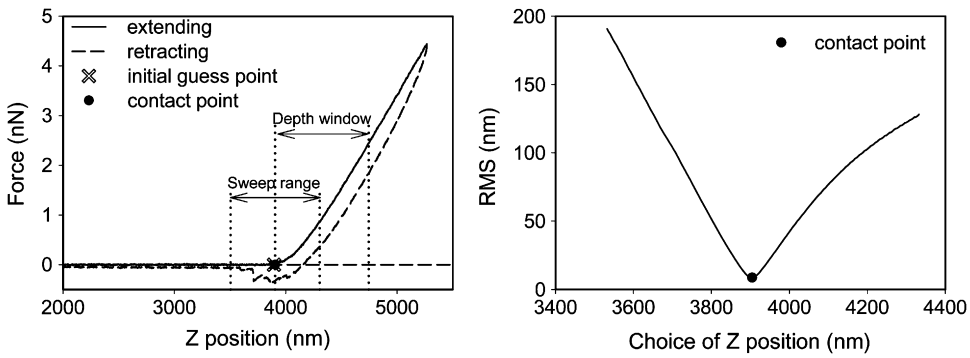

Fig. 1. Typical AFM data and root mean square error (RMS) plot. Left: a representative force–displacement curve, showing depth window, sweep range and initial contact point marked as dotted lines and a dot, respectively. Right: RMS error for the curve to the left as a function of the choice of contact point (z). Indentation was performed with a 2.5 μm sphere in saline.